Heteroatom–doped hollow carbon microspheres based on amphiphilic supramolecular vesicles and highly crosslinked polyphosphazene for high performance supercapacitor electrode materials

Kuiyong Chen[a], Xiaobin Huang[a*], Chaoying Wan[b], Hong Liu[a]

[a] School of Aeronautics and Astronautics, Shanghai Jiao Tong University, 800 Dongchuan Road, Shanghai, 200240, P R China.

[b] International Institute for Nanocomposites Manufacturing (IINM), WMG, University of Warwick, Coventry, CV4 7AL, UK.

*Corresponding author. E-mail: xbhuang@sjtu.edu.cn. Fax: +86-21-54741297, Tel: +86-21-54747142

Abstract

Hybrid hollow polymeric microspheres (HPMSs) are synthesized by encapsulating the supramolecular vesicles with polyphosphazene through a rapid one-step polycondensation reaction. Subsequent carbonization treatments of the HPMSs lead to corresponding hollow carbon microspheres (HCMSs) with well-preserved geometry. The sizes of HPMSs and HCMSs are controlled by the vesicles, which is directly determined by the feeding ratio of the assembly units. Electrodes based on HCMSs showed a specific capacitance of 314.6 F/g at a current density of 0.2 A/g in 6 M KOH electrolyte, 180.0 F/g at a current density of 30 A/g, and high stability of 98.2% of capacity retention after 2000 cycles. Both the high surface area and high heteroatoms level of HCMSs contribute to the excellent capacitive performance. Meanwhile, the hollow carbon structure ensured the satisfactory capacitive performance by increasing utilization efficiency of the surface area as well as achieving short diffusion paths for electrolyte ions.

Keywords: carbon; polyphosphazene; hollow microspheres; supercapacitor.

1. Introduction

Carbon micro-, nano-materials have been widely considered for use as electrode materials for energy storage devices, such as supercapacitors, batteries and fuel cell, due to their excellent electrical conductivity, stable physicochemical properties, low cost, and amenability to surface chemical modifications [1, 2]. Different types of carbon materials such as active carbon [3], carbon nanofibers [4, 5], carbon nanotubes [6, 7], graphene and its derivatives [8, 9], and mesoporous carbon [10] have been employed as electrode materials for supercapacitors, but the low energy density is the main technical challenge that limit the performance of the devices. The performance of supercapacitor electrodes depends intimately on the surface properties and conductivity of the carbon materials [1]. Carbon-based electrodes with higher specific surface area, porosity and higher electrical conductivity are favorable for increasing the capacity and energy density of the electrodes. On the other hand, carbon materials with special designed architecture could enhance the penetration and transportation efficiency of electrolyte ions, and thus can endow the electrodes with better electrochemical performance at high current densities [8, 11-13].

Hollow carbon microspheres (HCMSs) have been used as supercapacitor electrode materials due to their unique characteristics, including high surface utilization efficiency, short mass diffusion and low transport resistance [14-16]. Up to now, the fabrication of HCMSs is generally based on hard- or soft-template methods, which often require multiple steps and hazardous solvents to remove the templates and purify the products. In addition, the morphology regulation of HCMSs is dependent on the

availability of the templates [16-18]. Recently, hollow porous carbon spheres were synthesized through carbonization of porous organic frameworks [19]. The specific surface area could reach 525 m^2/g, with N-content of 4.73 at%. The as-assembled supercapacitor possessed a specific capacitance of 230 F/g at a current density of 0.5 A/g, and capacitance retention of ~98% after 1500 charge-discharge cycles. Hollow carbon nano-cocoons were also reported by carbonization of core/shell Fe_2O_3/carbon precursor at 850 ^oC, the hollow nano-cocoons based supercapacitor exhibited a capacitance of 220 F/g at a scan rate of 5 mV/s, and high stability with 98% of capacity maintance after 1000 cycles [20]. These results indicate the potential of hollow porous carbon structure for high performance supercapacitor electrode materials.

In this work, we report a novel yet facile method for synthesis of HCMSs containing high level of heteroatom. This is realized by taking the advantage of dynamic polyphosphazene chemistry which we have developed recently in synthesis of inorganic-organic hybrids with controlled morphology. Polyphosphazene is versatile in surface modification for nanomaterials, and hybrid materials such as silver nanocables wrapped with polyphosphazene, carbon nanotubes modified with polyphosphazene have been facilely synthesized[21-23]. Based on the polyphosphazene chemistry, first, amphiphilic supramolecular vesicles were synthesized through proton-transfer hydrogen bonding interactions [24]. Second, hybrid hollow polymeric microspheres (HPMSs) were synthesized via direct coating the vesicles with polyphosphazene through a rapid one-step polycondensation reaction. The morphology of HPMSs was controllable by simply adjusting the monomer ratios of the supramolecular vesicles,

thereby offering feasibility for tuning the hollow structure. Subsequent carbonization and activation processes leaded to heteroatom-doped hollow carbon microspheres. Electrochemical tests showed high capacitive performance of the HCMSs. This work offers a facile methodology for producing HCMSs, and used for high performance supercapacitor electrodes.

2. Materials and Methods

2.1 Materials

Hexachlorocyclotriphosphazene (HCCP) was synthesized as described in the literature[25], it was recrystallized from dry hexane and allowed to undergo two cycles of sublimation before use. Potassium hydroxide (KOH), trimethylamine (TEA), ethyl alcohol, and acetonitrile were purchased from Shanghai Chemical Reagents Corp. (Shanghai, China) and used as received. Acetylene black (50% compressed, >99.9% purity. 75 m^2/g specific area, 80–120 g/L bulk density) was purchased from Alfa Aesar. A polytetrafluoroethylene (PTFE) preparation suspension in water (60 wt% dispersion), 4,4'-thiobisbenzenethiol (MPS) and *p*-phenylenediamine (*p*-PDA) were purchased from Aladdin Industrial Corporation.

2.2. Preparation of vesicle based on MPS and TEA

The vesicle was prepared according to similar method described in our previous work[24]. Briefly, 1.00 g MPS was added to a 150 ml flask containing 60 ml acetonitrile. The solution was placed in an ultrasonic bath (150 W, 50 °C). After the MPS was solved, 1.00 ml of TEA was added to the solution. A white solution containing vesicle was

prepared. Furthermore, keep the feeding ratio of MPS and TEA unchanged, the vesicle solutions with various dosages of MPS and TEA were prepared. The vesicle solutions were denoted as MPS/TEA-D, where D represents the dosage of MPS (D=0.05, 0.10, 0.30, 1.00, 1.50 g).

2.3 Preparation of HPMSs

Hybrid HPMSs were simply synthesized via an in situ polycondensation reaction between HCCP and *p*-PDA in the vesicle solution. Typically, the prepared vesicle solution was transferred into an autoclave containing a certain amount of HCCP and *p*-PDA (with mass ratio m_{HCCP}: $m_{p\text{-}PDA}$: m_{MPS}=1:1:2). After addition of proper amount of TEA and saturated with nitrogen, the autoclave was sealed and maintained at 160 °C for 3 hours. The final product was washed with ethanol and water, respectively, and dried at 80 °C for 12 hours. The as prepared HPMSs were denoted as HPMS-D, where D represented the dosage of MPS in Part 2.2, with D=0.05, 0.10, 0.30, 1.00, 1.50 g, respectively.

2.4 **Preparation of HCMSs**

This process involved a carbonization process and a following activation process with KOH acted as activator. Both processes were conducted under nitrogen atmosphere. Typically, 0.30 g of HPMS-1.00 in a ceramic boat was putted in the furnace. The temperature was ramped to 350 °C with a heating rate of 5 °C/min. Followed by an isothermal process for 1 hours, the temperature was ramped to 500 °C at a heating rate of 5 °C/min, and kept at that value for 2 hours. Ultimately, the temperature was ramped to 800 °C with a heating rate of 5 °C/min. And then, the temperature was naturally

cooled to room temperature to obtain intermediate product. In the activation process, the intermediate product was mixed with KOH (with the mass ratio of KOH to intermediate product 3:1). The temperature was ramped to the desired value (550, 650, 750 °C) at a heating rate of 5 °C/min and then kept at that value for 2 h. Samples were collected when the resistance furnace was cooled to ambient temperature. Final products were denoted as HCMS-T, where T represents the maximum activation temperature (T=550, 650, 750 °C).

2.5. Characterization

Transmission electron microscopy (TEM) images were taken using a JEOL–2010 transmission electron microscope (Tokyo, Japan) at an acceleration voltage of 200 kV. Field–emission scanning electron microscopy (SEM) measurements were performed with a NOVA NANOSEM 450 field emission scanning electron microscope (FEI Company, Eindhoven, Netherlands). X–ray diffraction (XRD) measurements were carried out on a Bruker D8 Advance diffractometer using Cu Kα radiation. The instrument was operated at 40 kV and 40 mA, and the scanning was performed within the 2θ range of 10° to 80° at an interval of 6°/min. X–ray photoelectron spectroscopy (XPS) measurement was performed on a Kratos Axis Ultra DLD spectrometer using Al Kα X–ray radiation (hv =1486.6 eV) as the X–ray source for excitation, all of the XPS spectra were calibrated using the C1s peak at 284.8 eV as the standard. Raman spectra at 532 nm excitation wavelength were obtained by using a Nicolet Almega XR dispersive Raman spectrometer. Nitrogen adsorption and desorption isotherms at 77 K were recorded with an ASAP 2010 M+C surface analyzer (Micromeritics Inc., USA).

2.6. Electrochemical measurement

Electrochemical measurements were conducted by using a conventional three–electrode system. The working electrodes were fabricated by coating nickel foam substrates (1 cm×1 cm) with electrode slurry, which was obtained by mixing the sample with acetylene black–ethanol solution and the PTFE preparation in a mass ratio of 8:1:1. Subsequently, the coated substrates were dried at 100 °C for 12 h in a vacuum oven, and finally pressed under 10 MPa pressure. The typical mass loading of the active material on the electrode is 5 mg. Cyclic voltammetry (CV), galvanostatic charge/discharge and alternating–current (AC) impedance measurements were conducted on a CHI 660C electrochemical workstation (CH Instruments) by using Hg/HgO and platinum plate electrodes as reference and counter electrodes, respectively. A 6 M KOH aqueous solution was employed as the electrolyte.

3. Results and Discussion

HCMSs were prepared through a synthetic procedure depicted in Fig. 1. First, amphiphilic supramolecular vesicles were synthesized through proton-transfer hydrogen bonding via acid–base interaction following our previous work [24], and the vesicle size was adjustable by varying the assembly concentration of TEA and MPS. Next, HPMSs were synthesized via an in situ polycondensation reaction between HCCP and *p*-PDA in the presence of the vesicles. Generally, HCCP reacted with *p*-PDA to form polyphosphazene, with TEA acted as acid-acceptor. In the initial stage of the reaction, large numbers of nanometer-sized polyphosphazene particles were produced, and they conveniently diffused to the surface of the vesicles to coat the vesicles. With

the reaction progressed, polyphosphazene shell was formed, similar to our previous reports [21-23]. Fig. 2 shows TEM images of HPMSs synthesized in an ultrasonic bath with different assembly concentrations of TEA and MPS. As shown in Fig.2a, with the dosage of MPS and TEA being 0.05 g and 0.05 ml (in a 60 ml solution), respectively, solid vesicles were synthesized, therefore polymeric microspheres with diameter of approximately 400 nm were obtained. With the increase of the assembly concentration of MPS and TEA, hollow polymeric microspheres were formed and the size became bigger than the solid ones (Fig. 2b-e). With the increase of dosage of MPS and TEA to 1.00 g and 1.00 ml, larger HPMSs were obtained, with diameter about 1.5~2.5 μm (Fig. 2d). With the further increase of the dosage of MPS and TEA to 1.50 g and 1.50 ml, the morphology of the microspheres tended to be steady (Fig. 2e). These results indicate the obvious influence of the amphiphilic supramolecular vesicle templating on the morphology of the polymeric microspheres. It is feasible to tailor the morphology of the polymeric microspheres via controlling the assembly condition of the amphiphilic supramolecular vesicles. FTIR was used to characterize the molecular structure of the HPMSs (Fig. S1). The peak at 3068 cm^{-1} (a) is a stretching vibration peak of C-H bonds of the phenyl units. The characteristic absorptions at 1631 cm^{-1} (b) and 1532 cm^{-1} (d) are assigned to the phenyl absorption of the *p*-PDA units, the characteristic absorptions at 1576 cm^{-1} (c) and 1471 cm^{-1} (e) are assigned to the phenyl absorption of the MPS units. The characteristic peaks of the P=N and P–N in cyclotriphosphazene structure can be seen at 1164 cm^{-1} (f) and 949 cm^{-1} (g). The strong absorption peak of the P–Cl band of HCCP at 519 cm^{-1} and 602 cm^{-1} (h') disappeared after the polycondensation.

Meanwhile, the characteristic peak of P–N (in HCCP) band at 874 cm^{-1} shows a little blue shift to 949 cm^{-1} (g) in HPMSs, demonstrating the formation of new P–NH–(Ph) band. The results suggest the formation of highly crosslinked polyphosphazene (Fig. 2f), similar to the results shown in the previous reports [26-28].

HCMSs were prepared by carbonization and activation of HPMSs under inert atmospheres, and the samples derived from HPMS-1.00 (as shown in Fig.2d) were as the main research object. The samples were carbonized at 800 ^{o}C and further activated at three temperatures (550, 650 and 750 ^{o}C). As shown in Fig. 3, regular hollow spherical structure was well-preserved after the carbonization and activation process. HCMS-550 showed outer diameter about 0.5 μm and wall thickness about 100 nm, much smaller than those of the original HPMS-1.00, which are of diameter about 1.5 μm and wall thickness about 250 nm. Regular hollow structures were found in all the HCMSs samples that were activated at higher temperatures (Fig. S2). In comparing with HPMSs, the vesicles synthesized from TEA and MPS crashed and were fused together during the carbonization process (Fig. 3b). The results indicate the important function of the highly crosslinked polyphosphazene in preserving the hollow structure during the carbonization process.

The structure of HCMSs activated at various temperatures (550, 650 and 750 °C) were characterized by XRD and Raman spectroscopy. As shown in Fig. 4a, the broad diffraction peaks spanning the range of 22°-25° suggest typical turbostratic structures of the samples [29]. Raman spectrum is a powerful tool for identifying the structure of

carbon materials. In Fig.4b, the spectra show G line and D line signals at 1585 cm^{-1} and 1340 cm^{-1}, respectively. The D line is associated with the defects, curved sheets and dangling bonds in the carbon structure, while the G line corresponds to the E 2g mode of graphene.[30, 31] In general, the relative intensity of D line and G line (I_D/I_G) varies with the regularity of the structure and could be used to evaluate carbon materials[32]. The I_D/I_G ratios of HCMSs decreased slightly with the increase of activation temperature, indicating poor regularity level of the carbon materials activated at higher temperatures. That results may be due to in-plane C=C cracks at high temperature caused by the activation of KOH.

Nitrogen adsorption–desorption measurements were conducted to characterize the pore structure of HCMSs. Fig. 4c shows nitrogen adsorption–desorption isotherms of the samples activated at three temperatures. All of the samples exhibite type IV isothermals, and the large adsorption capacities in the relative low-pressure area suggest high level of micropores. The specific surface areas of the samples were calculated by Brunauer–Emmett–Teller (BET) method. HCMS-750 shows the highest BET surface area (2199 m^2/g) and pore volume (1.25 cm^3/g) than HCMS-550 and HCMS-650 (Table 1). Fig. 4d shows the pore size distribution curve of HCMSs. As can be seen, HCMSs mainly have the pore structure of micropores and mesopores, and HCMS-750 have the largest pore volume (detailed data is shown in Table 1).Wide–region–scanning XPS spectra are shown in Fig. 4e. High level of heteroatoms including C, N, O and S are detected on the surface of HCMSs. These heteroatoms come from the molecular

backbones of the HPMSs. The presence of heteroatoms in carbon structure has been demonstrated to be efficient in promoting the specific capacity [10, 12, 33-35]. As shown in Table 1, heteroatom level decreases with the increase of activation temperature, however, even after being activated at 750 °C, the heteroatom level of HCMS-750 still maintains as high as 11.5 at.%.

The binding configurations of C, N, O and S in the samples were also evaluated by XPS. The complex C1s spectra for HCMSs can be deconvoluted into three different peaks at the binding energies about 284.8, 285.8 and 288.5 eV, corresponding to graphite-like carbon (Sp2 C), C-O & C=N, C-O-C & C-N, respectively (Fig. 5a). The large amount of graphite-like carbon brings good electroconductivity to carbon materials[36]. The complex O 1s spectra for HCMSs can be deconvoluted into two different peaks at the binding energies about 531.5 and 533.0 eV, which can be mainly assigned to C=O (O1), C−O (O2) respectively (Fig.5b)[32, 37]. The peak centered at 400.3 eV (Fig. 5c) is assigned to pyrrolic N, which can enhance the pseudocapacitance of carbon material [38, 39]. The high resolution S2p peaks of HCMSs are resolved into three different peaks at the binding energies of 164.2, 165.4 and 168.8 eV. The former two peaks are in agreement with the 2p 3/2 (S1) and 2p 1/2 (S2) positions of thiophene-S, ant the third peak may arise from some oxidized sulfur (S3)[40]. It can be inferred that the sulfur is mainly doped at the edges and defects of carbon materials in the form of thiophene-like structures.

The capacitive performance of HCMSs was characterized through CV,

galvanostatic charge/discharge and AC impedance. CV was conducted in aqueous electrolyte of 6 M KOH within a potential window of -0.1 V to -0.9 V (vs. Hg/HgO). Fig. 6a shows cyclic voltammograms of HCMSs obtained at a scan rate of 2 mV/s. These curves show near rectangular shape, indicating ideal electric double-layer capacitive behavior [41]. The CV curves of the samples at different scan rates are shown in Fig. S3. HCMS-750 showed more regular rectangular shapes even at high scan rates, suggesting faster diffusion of the electrolyte[42]. It mainly benefited from the well-developed pore structure and high BET surface of HCMS-750 at higher activation temperature.

Galvanostatic charge–discharge experiments were conducted at various current densities in the potential window of -0.9 to -0.1 V (vs. Hg/HgO) to characterize the performance of the HCMS–based electrodes. Gravimetric capacitances of the samples were calculated according Equation (1) [43]:

$$C_g = (I \times \Delta t)/(2\mathrm{m} \times \Delta \mathrm{V}) \qquad (1)$$

where C_g is the specific capacitance of the sample, m is the mass of electroactive materials, I is the charge–discharge current, Δt is the time elapsed within one period of charge–discharge in the potential window of -0.9 to -0.1 V, and ΔV is the potential window. Fig. 6b shows the charge–discharge curves of HCMS–based electrodes at a current density of 0.2A/g. All curves show near–triangular shapes, reflecting ideal capacitive behaviour of the electrodes. As shown in Table S1, the C_g values of HCMS-550, HCMS-650 and HCMS-750 could reach as high as 314.6, 301.3 and 234.8 F/g at a current density of 0.2 A/g, respectively. Area–

specific capacitances (C_{sa}) normalized to the BET surfaces area were also calculated. At current density of 0.2 A/g, HCMS-550, HCMS-650 and HCMS-750 show C_{sa} about 0.279 F/m^2, 0.181 F/m^2, 0.107 F/m^2, respectively. Although HCMS-550 shows the lowest BET surface area, however, due to the high heteroatom level, which can bring pseudocapacitance effect, HCMS-550 shows the highest specific capacitance. With the raise of the activation temperature, the BET surface of the samples increased rapidly, however, the heteroatom level decreased, thus the capacitance of HCMS-650 and HCMS-750 decreased.

Charge–discharge curves of HCMSs obtained at various current densities are shown in Fig. S4. The specific capacitances of HCMSs at various current densities were calculated through Equation (1), and the results are presented in Fig. 6c. As the applied current density was increased from 0.2 A/g to 10 A/g, the capacitance retention ($=C_{g\ (10\ A/g)}/C_{g\ (0.2\ A/g)}\times 100\%$) of HCMS-550, HCMS-650, and HCMS-750 reached 76.1%, 77.2%, and 84.1%, respectively. The highest capacitance retention of HCMS-750 may be due to well develop pore structure at high activation temperature. The well-developed pore structure would be efficient to reduce the transition resistance of the ions. Even when the current density reached 30 A/g, the specific capacitance of HCMS-550 and HCMS-650 could reach as high as 180.0 F/g and 183.8 F/g, respectively, showing high-rate charge-discharge performance.

The variation of electrochemical impedance spectra of HCMSs is depicted in Fig. 6d. All curves display two parts, namely, roughly semicircle portions in the high-

frequency range and straight lines in the low-frequency range. Generally, the semicircle in the high–frequency region represents an electrochemistry–controlled process, and the straight line in the low–frequency responds to the electrolyte ion diffusion–controlled reaction. The intercept at the real impedance axis in the high-frequency region is related to internal resistance, which includes the resistance of the bulk electrolyte, the intrinsic resistance of HCMSs, and contact resistance at the interface of HCMSs/Ni foam current collector. The internal resistance values of HCMS-550, HCMS-650 and HCMS-750 are in the range of 0.53, 0.60 and 0.61 Ω, indicating low resistance for electrolyte transport between the reference and working electrodes. The semicircle diameter reflects the magnitude of charge transfer resistance (R_{ct}) caused by Faradic reactions and EDLC at the electrode/electrolyte interface. HCMS-550, HCMS-650 and HCMS-750 show similar R_{ct} about 0.21Ω. The low frequency straight line is related to the ion diffusion resistance in the electrode materials. The low frequency straight line of HCMS-750 shows the largest slop. This should be a consequence of the well-developed pore structure and the large BET surface area active at higher temperature, which are more efficient for ion transport.

The cycling durability of HCMS-550 in 6 M aqueous KOH electrolyte was characterized through galvanostatic charge–discharge experiments with a current density 10 A/g. As shown in Fig. 6e, the specific capacitance of HCMS-550 nearly remains constant, and the capacitive retention ratio was more than 98.2% after 2000 cycles.

4. Conclusions

A facile process for synthesis of HPMSs and HCMSs is presented. By controlling the formation condition of the amphiphilic supramolecular vesicles, the morphology of HPMSs can be facilely controlled. The highly crosslinked structure of polyphosphazene is crucial to preserve the hollow structure in the carbonization process. HCMSs with high specific surface area (1128-2199 m^2/g), pore volume (0.56-1.25 m^2/g) and in particular, high heteroatoms doping (11.5-14.41 at%) exhibit excellent capacitive performance in 6 M KOH electrolyte. Take the HCMS-550 for example, a specific capacitance of 314.6 F/g at a current density of 0.2 A/g, and 180.0 F/g at a current density of 30 A/g are obtained. The excellent capacitive performance benefits from the high surface area and high content of heteroatoms, as well as the well-developed pore structure that allows short diffusion paths for electrolyte ions. This work provides a facile method for synthesis hollow carbon microspheres for high performance supercapacitors.

Acknowledgements

This work was supported by the Natural Science Foundation of China [grant numbers 21274092, 51133003, 61376003, 91441205]; and Shanghai Science & Technology Committee [grant numbers 10ZR1416100].

References

[1] G. Wang, L. Zhang, J. Zhang, A review of electrode materials for electrochemical supercapacitors, Chemical Society Reviews, 41 (2012) 797-828.

[2] T. Lin, I.-W. Chen, F. Liu, C. Yang, H. Bi, F. Xu, F. Huang, Nitrogen-doped mesoporous carbon of extraordinary capacitance for electrochemical energy storage, Science, 350 (2015) 1508-1513.

[3] J. Gamby, P.L. Taberna, P. Simon, J.F. Fauvarque, M. Chesneau, Studies and characterisations of various activated carbons used for carbon/carbon supercapacitors, Journal of Power Sources, 101 (2001) 109-116.
[4] L.-F. Chen, X.-D. Zhang, H.-W. Liang, M. Kong, Q.-F. Guan, P. Chen, Z.-Y. Wu, S.-H. Yu, Synthesis of Nitrogen-Doped Porous Carbon Nanofibers as an Efficient Electrode Material for Supercapacitors, ACS Nano, 6 (2012) 7092-7102.
[5] B. Xu, F. Wu, R. Chen, G. Cao, S. Chen, Y. Yang, Mesoporous activated carbon fiber as electrode material for high-performance electrochemical double layer capacitors with ionic liquid electrolyte, Journal of Power Sources, 195 (2010) 2118-2124.
[6] F. Picó, J.M. Rojo, M.L. Sanjuán, A. Ansón, A.M. Benito, M.A. Callejas, W.K. Maser, M.T. Martínez, Single-Walled Carbon Nanotubes as Electrodes in Supercapacitors, Journal of The Electrochemical Society, 151 (2004) A831-A837.
[7] Y. Rangom, X. Tang, L.F. Nazar, Carbon Nanotube-Based Supercapacitors with Excellent ac Line Filtering and Rate Capability via Improved Interfacial Impedance, ACS Nano, 9 (2015) 7248-7255.
[8] H. Luo, Z. Liu, L. Chao, X. Wu, X. Lei, Z. Chang, X. Sun, Synthesis of hierarchical porous N-doped sandwich-type carbon composites as high-performance supercapacitor electrodes, Journal of Materials Chemistry A, 3 (2015) 3667-3675.
[9] M. Lee, B.H. Wee, J.D. Hong, High Performance Flexible Supercapacitor Electrodes Composed of Ultralarge Graphene Sheets and Vanadium Dioxide, Advanced Energy Materials, 5 (2015).
[10] Q. Shi, R. Zhang, Y. Lv, Y. Deng, A.A. Elzatahrya, D. Zhao, Nitrogen-doped ordered mesoporous carbons based on cyanamide as the dopant for supercapacitor, Carbon, 84 (2015) 335-346.
[11] S. Dutta, A. Bhaumik, K.C.W. Wu, Hierarchically porous carbon derived from polymers and biomass: effect of interconnected pores on energy applications, Energy & Environmental Science, 7 (2014) 3574-3592.
[12] L.-F. Chen, Z.-H. Huang, H.-W. Liang, H.-L. Gao, S.-H. Yu, Three-Dimensional Heteroatom-Doped Carbon Nanofiber Networks Derived from Bacterial Cellulose for Supercapacitors, Advanced Functional Materials, 24 (2014) 5104-5111.
[13] Z. Yu, L. Tetard, L. Zhai, J. Thomas, Supercapacitor electrode materials: nanostructures from 0 to 3 dimensions, Energy & Environmental Science, 8 (2015) 702-730.
[14] F. Ma, H. Zhao, L. Sun, Q. Li, L. Huo, T. Xia, S. Gao, G. Pang, Z. Shi, S. Feng, A facile route for nitrogen-doped hollow graphitic carbon spheres with superior performance in supercapacitors, Journal of Materials Chemistry, 22 (2012) 13464-13468.
[15] X. Fang, J. Zang, X. Wang, M.-S. Zheng, N. Zheng, A multiple coating route to hollow carbon spheres with foam-like shells and their applications in supercapacitor and confined catalysis, Journal of Materials Chemistry A, 2 (2014) 6191-6197.
[16] J. Han, G. Xu, B. Ding, J. Pan, H. Dou, D.R. MacFarlane, Porous nitrogen-doped hollow carbon spheres derived from polyaniline for high performance supercapacitors, Journal of Materials Chemistry A, 2 (2014) 5352-5357.
[17] R. Liu, S.M. Mahurin, C. Li, R.R. Unocic, J.C. Idrobo, H. Gao, S.J. Pennycook, S. Dai, Dopamine as a Carbon Source: The Controlled Synthesis of Hollow Carbon Spheres and Yolk-Structured Carbon Nanocomposites, Angewandte Chemie, 123 (2011) 6931-6934.
[18] C. Zhang, H.B. Wu, C. Yuan, Z. Guo, X.W. Lou, Confining Sulfur in Double-Shelled Hollow Carbon Spheres for Lithium–Sulfur Batteries, Angewandte Chemie, 124 (2012) 9730-9733.
[19] X. Liu, L. Zhou, Y. Zhao, L. Bian, X. Feng, Q. Pu, Hollow, Spherical Nitrogen-Rich Porous Carbon

Shells Obtained from a Porous Organic Framework for the Supercapacitor, ACS Applied Materials & Interfaces, 5 (2013) 10280-10287.
[20] J. Zhang, K. Wang, S. Guo, S. Wang, Z. Liang, Z. Chen, J. Fu, Q. Xu, One-Step Carbonization Synthesis of Hollow Carbon Nanococoons with Multimodal Pores and Their Enhanced Electrochemical Performance for Supercapacitors, ACS Applied Materials & Interfaces, 6 (2014) 2192-2198.
[21] J. Fu, X. Huang, Y. Huang, J. Zhang, X. Tang, One-pot noncovalent method to functionalize multi-walled carbon nanotubes using cyclomatrix-type polyphosphazenes, Chemical Communications, (2009) 1049-1051.
[22] J. Fu, X. Huang, Y. Huang, Y. Pan, Y. Zhu, X. Tang, Preparation of Silver Nanocables Wrapped with Highly Cross-Linked Organic-Inorganic Hybrid Polyphosphazenes via a Hard-Template Approach, The Journal of Physical Chemistry C, 112 (2008) 16840-16844.
[23] X. Huang, W. Wei, X. Zhao, X. Tang, Novel preparation of polyphosphazene-coated carbon nanotubes as a Pt catalyst support, Chemical Communications, 46 (2010) 8848-8850.
[24] C. Shan, X. Huang, H. Wei, W. Wei, H. Sun, X. Tang, Micelle and vesicle formation from supramolecular complexes based on proton-transfer hydrogen bonding, RSC Advances, 4 (2014) 11216-11218.
[25] R.D. Jaeger, M. Gleria, Poly(organophosphazene)s and related compounds: Synthesis, properties and applications, Progress in Polymer Science, 23 (1998) 179-276.
[26] W. Wei, R. Lu, S. Tang, X. Liu, Highly cross-linked fluorescent poly(cyclotriphosphazene-co-curcumin) microspheres for the selective detection of picric acid in solution phase, Journal of Materials Chemistry A, 3 (2015) 4604-4611.
[27] W. Wei, R. Lu, H. Xie, Y. Zhang, X. Bai, L. Gu, R. Da, X. Liu, Selective adsorption and separation of dyes from an aqueous solution on organic-inorganic hybrid cyclomatrix polyphosphazene submicro-spheres, Journal of Materials Chemistry A, 3 (2015) 4314-4322.
[28] K. Chen, X. Huang, C. Wan, H. Liu, Heteroatom-doped mesoporous carbon nanofibers based on highly cross-linked hybrid polymeric nanofibers: Facile synthesis and application in an electrochemical supercapacitor, Materials Chemistry and Physics, 164 (2015) 85-90.
[29] H. Guo, Q. Gao, Boron and nitrogen co-doped porous carbon and its enhanced properties as supercapacitor, Journal of Power Sources, 186 (2009) 551-556.
[30] Z. Wen, S. Ci, F. Zhang, X. Feng, S. Cui, S. Mao, S. Luo, Z. He, J. Chen, Nitrogen-Enriched Core-Shell Structured Fe/Fe3C-C Nanorods as Advanced Electrocatalysts for Oxygen Reduction Reaction, Advanced Materials, 24 (2012) 1399-1404.
[31] G. Yang, H. Han, T. Li, C. Du, Synthesis of nitrogen-doped porous graphitic carbons using nano-CaCO3 as template, graphitization catalyst, and activating agent, Carbon, 50 (2012) 3753-3765.
[32] C. Wang, Y. Zhou, L. Sun, Q. Zhao, X. Zhang, P. Wan, J. Qiu, N/P-Codoped Thermally Reduced Graphene for High-Performance Supercapacitor Applications, The Journal of Physical Chemistry C, 117 (2013) 14912-14919.
[33] J. Han, L.L. Zhang, S. Lee, J. Oh, K.-S. Lee, J.R. Potts, J. Ji, X. Zhao, R.S. Ruoff, S. Park, Generation of B-Doped Graphene Nanoplatelets Using a Solution Process and Their Supercapacitor Applications, ACS Nano, 7 (2013) 19-26.
[34] W. Chen, J. Shi, T. Zhu, Q. Wang, J. Qiao, J. Zhang, Preparation of Nitrogen and Sulfur dual-doped Mesoporous Carbon for Supercapacitor Electrodes with Long Cycle Stability, Electrochimica Acta, 177 (2015) 327-334.
[35] K. Fujisawa, R. Cruz-Silva, K.-S. Yang, Y.A. Kim, T. Hayashi, M. Endo, M. Terrones, M.S.

Dresselhaus, Importance of open, heteroatom-decorated edges in chemically doped-graphene for supercapacitor applications, Journal of Materials Chemistry A, 2 (2014) 9532-9540.
[36] K. Ai, Y. Liu, C. Ruan, L. Lu, G. Lu, Sp2 C-Dominant N-Doped Carbon Sub-micrometer Spheres with a Tunable Size: A Versatile Platform for Highly Efficient Oxygen-Reduction Catalysts, Advanced Materials, 25 (2013) 998-1003.
[37] D. Hulicova-Jurcakova, M. Seredych, Q.L. Gao, T.J. Bandosz, Combined Effect of Nitrogen- and Oxygen-Containing Functional Groups of Microporous Activated Carbon on its Electrochemical Performance in Supercapacitors, Advanced Functional Materials, 19 (2009) 438–447.
[38] N. Daems, X. Sheng, I.J. Vankelecom, P. Pescarmona, Metal-free doped carbon materials as electrocatalysts for the oxygen reduction reaction, Journal of Materials Chemistry A, 2 (2014) 4085-4110.
[39] Y. Liao, Y. Huang, D. Shu, Y. Zhong, J. Hao, C. He, J. Zhong, X. Song, Three-dimensional nitrogen-doped graphene hydrogels prepared via hydrothermal synthesis as high-performance supercapacitor materials, Electrochimica Acta, 194 (2016) 136-142.
[40] S. Yang, L. Zhi, K. Tang, X. Feng, J. Maier, K. Müllen, Efficient Synthesis of Heteroatom (N or S)- Doped Graphene Based on Ultrathin Graphene Oxide- Porous Silica Sheets for Oxygen Reduction Reactions, Advanced Functional Materials, 22 (2012) 3634–3640.
[41] S. Bose, T. Kuila, A.K. Mishra, R. Rajasekar, N.H. Kim, J.H. Lee, Carbon-based nanostructured materials and their composites as supercapacitor electrodes, Journal of Materials Chemistry, 22 (2012) 767-784.
[42] S. Bose, T. Kuila, A.K. Mishra, R. Rajasekar, N.H. Kim, J.H. Lee, Carbon-based nanostructured materials and their composites as supercapacitor electrodes, Journal of Materials Chemistry, 22 (2011) 767-784.
[43] B.E. Conway, Electrochemical supercapacitors, Kluwer Academic /Plenum Publishers, New York (1999).

Figure Captions

Fig. 1 Scheme for the preparation of HCMSs based on amphiphilic supramolecular vesicles.

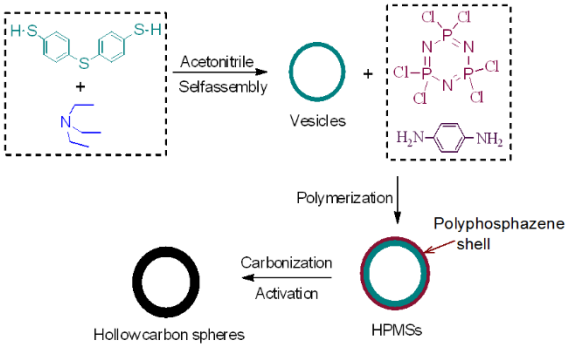

Fig. 2 TEM images of HPMS-0.05 (a), HPMS-0.10 (b), HPMS-0.30 (c), HPMS-1.00 (d), HPMS-1.50 (e). (f) Highly crosslinked molecular structure of polyphosphazene.

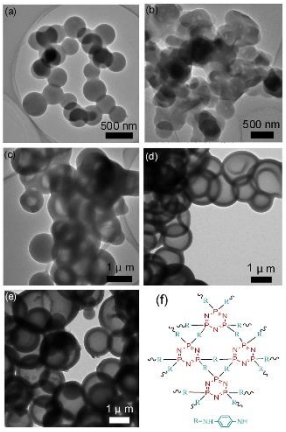

Fig. 3 (a) TEM images of HCMS-550, (b) SEM image of vesicles carbonized at 800 °C.

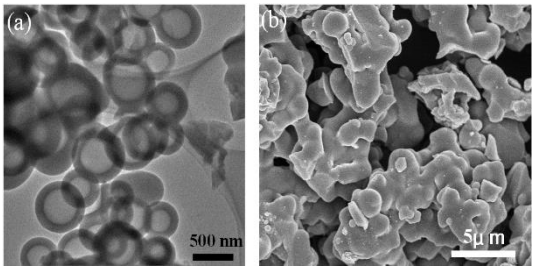

Fig. 4 Characterisation of structures of HCMSs activated at three temperatures: (a) XRD spectra of HCMSs; (b) Raman spectra of HCMSs; (c) Nitrogen adsorption–desorption isotherms of HCMSs; (d) Pore size distribution of HCMSs; (e) Wide–survey XPS spectra of HCMSs.

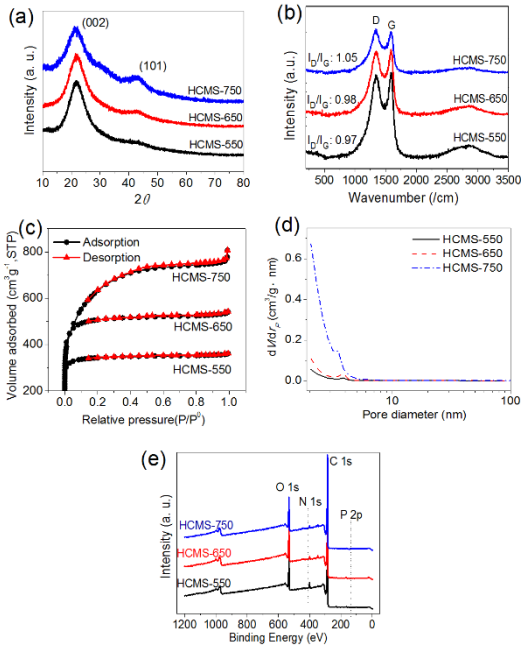

Fig. 5 High-resolution of C1s, N1s, O1s and S2p XPS spectra of HCMSs activated at various temperatures.

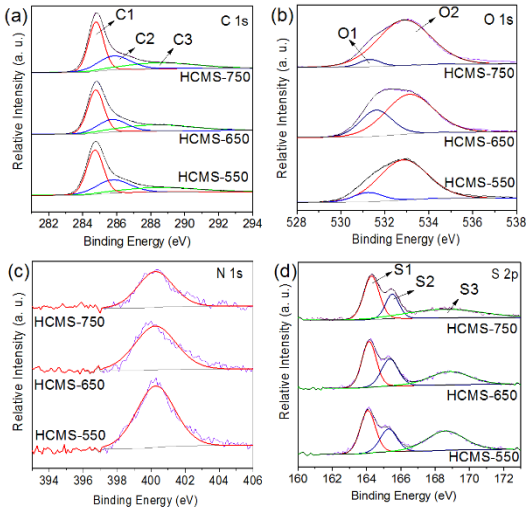

Fig. 6 (a) CV curves of HMCMs at a scan rate of 2 mV/s. (b) charge–discharge curves obtained at a current density of 0.2 A/g. (c) capacitance retention as a function of the current density. (d) Nyquist plots of HCMSs. The insert shows a magnified view in the high-frequency range. (e) cyclic performances of HCMS–550 electrode at a current density of 10 A/g.

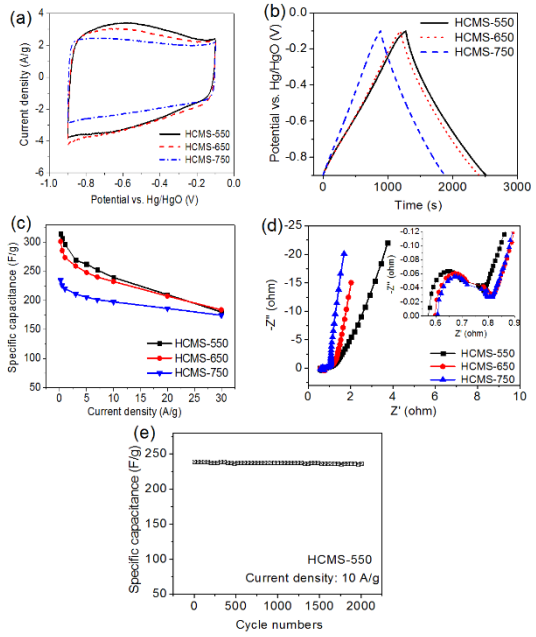

Table 1 Compositional properties, BET surface area and pore volume of HCMSs prepared via activation at various temperatures.

Sample	C (at.%)	N (at.%)	O (at.%)	P (at.%)	S (at.%)	S_{BET} m^2/g	V_{pore} cm^3/g
HCMS-550	85.59	2.21	11.50	0	0.70	1128.0	0.56
HCMS-650	87.51	2.05	9.68	0	0.76	1666.2	0.84
HCMS-750	88.47	1.20	9.79	0	0.54	2199.0	1.25